

# Scalarized neutron stars in massive scalar-tensor gravity: X-ray pulsars and tidal deformability

Zexin Hu,<sup>1</sup> Yong Gao,<sup>2,3,\*</sup> Rui Xu,<sup>3</sup> and Lijing Shao<sup>3,4,5,†</sup>

<sup>1</sup>*School of Physics, Peking University, Beijing 100871, China*

<sup>2</sup>*Department of Astronomy, School of Physics, Peking University, Beijing 100871, China*

<sup>3</sup>*Kavli Institute for Astronomy and Astrophysics, Peking University, Beijing 100871, China*

<sup>4</sup>*Max-Planck-Institut für Radioastronomie, Auf dem Hügel 69, D-53121 Bonn, Germany*

<sup>5</sup>*National Astronomical Observatories, Chinese Academy of Sciences, Beijing 100012, China*

(Dated: September 29, 2021)

Neutron stars (NSs) in scalar-tensor theories of gravitation with the phenomenon of spontaneous scalarization can develop significant deviations from general relativity. Cases with a massless scalar were studied widely. Here we compare the NS scalarizations in the Damour–Esposito-Farèse theory, the Mendes-Ortiz theory, and the  $\xi$ -theory with a massive scalar field. Numerical solutions for slowly rotating NSs are obtained. They are used to construct the X-ray pulse profiles of a pair of extended hot spots on the surface of NSs. We also calculate the tidal deformability for NSs with spontaneous scalarization which is done for the first time with a massive scalar field. We show the universal relation between the moment of inertia and the tidal deformability. The X-ray pulse profiles, the tidal deformability, and the universal relation may help to constrain the massive scalar-tensor theories in X-ray and gravitational-wave observations of NSs, including the Neutron star Interior Composition Explorer (NICER) satellite, Square Kilometre Array (SKA) telescope, and LIGO/Virgo/KAGRA laser interferometers.

## I. INTRODUCTION

Scalar-tensor (ST) theories of gravitation are the simplest extension to general relativity (GR) by adding real scalar fields which mediate gravity in part [1]. The properties of these theories depend on how the scalar fields couple with the metric and matters, as well as the potential term of scalars in the action. It has been demonstrated that for some choices of the coupling, the theories provide solutions which are close enough to GR in the weak-field regime while predict large differences in the strong-field regime [2–5]. Therefore, it is particularly interesting to study those kinds of ST theories since they provide explicit examples of large deviations from GR in the non-perturbative regime while still satisfy all experimental and observational bounds from weak-field experiments [6]. One well-studied set of the ST theories with such properties are characterized by a phenomenon called *spontaneous scalarization* [2]. In this work we will focus on neutron stars (NSs), which are strong-field systems available to astrophysical observations and possess matters with extreme densities and pressures [7–10] which are coupled to the scalar fields in the ST theories.

First discovered by Damour and Esposito-Farèse (DEF) in a mono-scalar ST theory, spontaneous scalarization can lead to non-perturbative, order-of-unity deviations from GR [2], as the scalar-field vacuum becomes unstable to the growth of the field in the presence of highly compact objects like NSs. We will focus on the specific class of ST theories where only one scalar field exists, and we focus on investigations with NSs. As we discuss in detail in Sec. II, spontaneous scalarization for NSs can also be understood as a Landau’s phase transition with the star’s baryonic mass taken as the control parameter [3, 11, 12]. For a sufficiently compact NS, the solution

with a nontrivial scalar field is energetically favored than the unstable solution that is composed of the GR metric and a vanishing scalar field.

The main motivation to study scalarized NSs is that they provide a new avenue to test gravity theories in the strong-field regime. For asymmetric binary pulsar systems, scalarized NSs can trigger the gravitational dipole radiation in ST theories [3, 7]. The dipole radiation will make the orbital energy loss faster than that in GR if there exists such an extra scalar degree of freedom, which in turn can be constrained by pulsar timing observations [3]. Besides, gravitational waves (GWs) from binary NS mergers have been directly detected with laser interferometers [13] and can be analyzed to test the dipole radiation [14–18] and put constraints on ST theories.

Most early studies of the ST theories with spontaneous scalarization considered a massless scalar field. However, observations of the pulsar–white dwarf orbital decay due to gravitational dipole radiation have constrained the parameter space of the massless ST theories stringently [7, 19–22]. Moreover, with a massless scalar field, the whole Universe could have been scalarized, which is clearly ruled out by the combination of Solar-system and cosmological observations [23]. A simple and natural way to avoid these difficulties is to consider a massive scalar field rather than a massless one [3, 24, 25]. Due to the mass term, the scalar field outside the star suffers a Yukawa-type suppression such that the scalar field’s contribution to the gravitational radiation can be effectively effaced. Therefore, much of the parameter space for massive ST theories is still not excluded by the pulsar timing observations [26, 27]. Besides, even a very light mass of the scalar field can prevent the scalarization of the Universe.

Different coupling functions between the scalar field and matters correspond to different kinds of ST theories. Currently, the DEF theory [2, 3], the Mendes-Ortiz (MO) theory [4, 28], and the  $\xi$ -theory [3, 29] are commonly used and all of them can lead to spontaneous scalarization of NSs. The DEF theory provides the simplest coupling function pos-

\* Corresponding author: [gaoyong.physics@pku.edu.cn](mailto:gaoyong.physics@pku.edu.cn)

† Corresponding author: [lishao@pku.edu.cn](mailto:lishao@pku.edu.cn)

sessing the spontaneous scalarization effect, and it is the most commonly studied ST theory since the seminal work by Damour and Esposito-Farèse [2, 3]. The  $\xi$ -theory is a well-motivated theory, which arises from inflationary models where  $\xi$  represents a dimensionless coupling constant in the Lagrangian [30]. However, the explicit form of the  $\xi$ -theory in the Einstein frame is not convenient for calculation. Therefore Mendes and Ortiz [4] constructed an analytical approximation of the  $\xi$ -theory, which is the so-called MO theory. After adding the mass term for the scalar field, the phenomenon of spontaneous scalarization still exists for all of those theories [4, 24, 29]. In this work, we calculate and compare the structure of a slowly rotating NS, and its macroscopic properties, including the mass-radius relation, the moment of inertia, and the tidal deformability, in the DEF, MO, and  $\xi$  theories. We also give explanations to the common features shown in spontaneous scalarization. The study serves as a comprehensive comparison between different ST theories with a massive scalar field, and discusses the relevance to a couple of current and near-future observations.

As we mentioned before, the massive ST theories are poorly constrained by the pulsar–white dwarf binary systems [19–22] due to the Yukawa-type suppression of the scalar field. However, the structure of scalarized NSs (e.g., mass and radius) in ST theories can still be very different from that in GR. Therefore, one possible method to constrain the parameter space of the massive ST theories is using the mass-radius relation (see e.g., discussions in Sec. 7 of Ref. [31]). Moreover, as discussed by Silva and Yunes [32], it is possible to perform strong-gravity tests with X-ray observations using a recently developed pulse profile model beyond general relativity. The X-ray pulse profiles from hot spots on the surface of a NS will be different in ST theories from those in GR because of both the difference in the mass-radius relation and the difference in the lightlike geodesic [33, 34].

We expect the theories in consideration to be constrained by the X-ray timing data from the ongoing Neutron star Interior Composition Explorer (NICER) program (see e.g., recent results in Refs. [35, 36]), and future planned X-ray satellites like THESEUS [37]. As an application of the numerical results of the scalarized NSs, we follow Refs. [29, 33] to calculate the X-ray pulse profiles of NSs with spontaneous scalarization and generalize their results to the case of extended hot spots for massive ST theories.

GW observations from binary NSs can also give constraints on massive ST theories. For coalescing binary NSs, the size of the stars cannot be ignored at the end of inspiral as they will be deformed in the tidal fields of their companions, and the deformation of each star contributes a correction to the waveform’s phasing [38]. A remarkable GW discovery of a binary NS system is GW170817 by the LIGO/Virgo detector network, where analysis has been performed to extract a constraint for the tidal deformability from the data [13, 39]. In Ref. [40], the tidal deformability of NSs in massless DEF theories is calculated, and it is shown that the deviation from GR can be large in some parameter space. In this work, we calculate the tidal deformability of NSs in massive ST theories which, to our knowledge, is done for the first time.

Discovered by Yagi and Yunes [41, 42], the dimensionless moment of inertia, the tidal deformability, and the spin-induced quadrupole moment of slowly rotating NSs in GR satisfy nearly universal relations which do not depend on the NSs’ equation of state (EOS). It has been found that in many other alternatives to GR the relations still hold with a high accuracy. The universal relations in massless ST theories have been shown by Pani and Berti [40], and for the viable parameter space of the theories, the deviation from GR is lower than 2%. Nevertheless, the universal relations may still be an interesting method to help us discriminate between GR and the ST theories without the detailed knowledge of the realistic EOS of NSs. In this work, we will discuss the universal relation between the moment of inertia and the tidal deformability in massive ST theories for the first time.

The organization of the paper is as follows. In Sec. II we briefly introduce the massive ST theories considered in this paper and give a discussion about the spontaneous scalarization. The differential equations for a slowly rotating NS are derived in Sec. III and the numerical solutions of NSs’ structure are also displayed there. As an application of the results, in Sec. IV we show the X-ray pulse profiles from a pair of hot spots on the surface of a scalarized NS. In Sec. V, the tidal deformability of a scalarized NS is calculated by considering a perturbation both in the metric and the scalar field. Then, we show the relation between the moment of inertia and the tidal deformability in Sec. VI. Finally, we summarize the paper in Sec. VII.

Throughout this work, we use the geometrized unit system where the “bare” gravitational constant  $G$  and the speed of light  $c$  are set to 1, except when traditional units are written out explicitly. The convention of the metric is  $(-, +, +, +)$ .

## II. MASSIVE SCALAR-TENSOR THEORIES

The action of a massive ST theory in the Einstein frame reads [3, 28, 43],

$$S = \frac{1}{16\pi} \int d^4x \sqrt{-g} \left[ R - 2g^{\mu\nu} \partial_\mu \varphi \partial_\nu \varphi - V(\varphi) \right] + S_m \left[ \Psi_m, A^2(\varphi) g_{\mu\nu} \right], \quad (1)$$

where  $R$  is the curvature scalar constructed from the metric  $g_{\mu\nu}$ ,  $\varphi$  is the scalar field coupled with the metric and matters, and  $S_m$  is the action of conventional matters where  $\Psi_m$  represents matter fields collectively. It is convenient to formulate the field equations via the metric  $g_{\mu\nu}$  in the Einstein frame, while matters are directly coupled to the Jordan frame metric  $\tilde{g}_{\mu\nu}$ , which is related to the Einstein metric  $g_{\mu\nu}$  via a conformal transformation  $\tilde{g}_{\mu\nu} = A^2(\varphi) g_{\mu\nu}$ . Jordan frame metric is the one measured by experiments. For this reason, the Jordan frame is usually referred to as the physical frame.

We take the scalar potential  $V(\varphi)$  as

$$V(\varphi) = 2m_\varphi^2 \varphi^2, \quad (2)$$

which represents a scalar field with a constant scalar mass  $m_\varphi$  in the Einstein frame. The corresponding Compton wave-

length of the scalar field is defined as

$$\lambda_\varphi = \frac{2\pi\hbar}{m_\varphi}, \quad (3)$$

where  $\hbar$  is the reduced Planck constant. We will use the reduced wavelength  $\lambda_\varphi \equiv \lambda_\varphi/2\pi$  in the rest of the work.

By varying the total action in Eq. (1) with respect to the tensor field  $g_{\mu\nu}$  and the scalar field  $\varphi$ , one obtains the field equations [1]

$$R_{\mu\nu} = 2\partial_\mu\varphi\partial_\nu\varphi + \frac{1}{2}g_{\mu\nu}V(\varphi) + 8\pi\left(T_{\mu\nu} - \frac{1}{2}g_{\mu\nu}T\right), \quad (4)$$

$$\square\varphi = \frac{1}{4}\frac{dV(\varphi)}{d\varphi} - 4\pi\frac{d\ln A(\varphi)}{d\varphi}T. \quad (5)$$

Note that all tensorial operations in Eqs. (4–5) are performed in the Einstein frame.  $T_{\mu\nu}$  is the energy-momentum tensor for conventional matters, which is defined as  $T_{\mu\nu} \equiv -2(-g)^{-1/2}\delta S_m/\delta g^{\mu\nu}$ . While the energy-momentum tensor in the physical frame can be represented as  $\tilde{T}_{\mu\nu} \equiv -2(-\tilde{g})^{-1/2}\delta S_m/\delta\tilde{g}^{\mu\nu} = A^{-2}T_{\mu\nu}$ , which satisfies the conservation equation  $\tilde{\nabla}_\nu\tilde{T}^{\mu\nu} = 0$ . For an ideal fluid, the energy-momentum tensor in the physical frame is

$$\tilde{T}^{\mu\nu} = (\tilde{\epsilon} + \tilde{p})\tilde{u}^\mu\tilde{u}^\nu + \tilde{g}^{\mu\nu}\tilde{p}. \quad (6)$$

As commonly used in the literature, we define  $\alpha(\varphi) \equiv d\ln A(\varphi)/d\varphi$ . From Eq. (5), it is clear that  $\alpha(\varphi)$  plays the role of measuring the field-dependent coupling strength between the scalar field and matters. Generally, we expand  $\ln A(\varphi)$  around a background scalar field  $\varphi_0$ ,

$$\ln A(\varphi) = \ln A(\varphi_0) + \alpha_0(\varphi - \varphi_0) + \frac{1}{2}\beta_0(\varphi - \varphi_0)^2 + \dots, \quad (7)$$

where  $\varphi_0$  denotes the asymptotic value of  $\varphi$  at spatial infinity. In the theories with a massless scalar field, all the post-Newtonian parameters are proportional to powers of  $\alpha_0$  [2], and the Solar system experiments have constrained  $\alpha_0$  very close to zero [6], which indicates a very weak coupling between matters and the scalar field in the weak-field regime. The quadratic coefficient  $\beta_0$  is nearly not constrained by Solar system experiments since it enters in the post-Newtonian expansion with a multiplier of  $\alpha_0^2$ , and thus is always suppressed by the already well constrained coefficient  $\alpha_0$ . In this work, with a massive scalar, the asymptotic value  $\varphi_0$  has to be zero due to the scalar potential in Eq. (2), and we take  $A(\varphi_0) = 1$  and  $\alpha_0 = 0$  for simplicity.

Currently, there are three main representative forms for the function  $\alpha(\varphi)$  that can lead to spontaneous scalarization. We will describe these theories as follows.

In the DEF theory [2, 3], the function form of the conformal factor is

$$A(\varphi) = e^{\frac{1}{2}\beta(\varphi-\varphi_0)^2}, \quad (8)$$

which provides the coupling function

$$\alpha(\varphi) = \beta(\varphi - \varphi_0). \quad (9)$$

This coupling function is linear in  $\varphi$  and can give large deviations from GR in the strong-field regime due to the positive correlation between the coupling strength and the scalar field.

A well-motivated form of  $A(\varphi)$  from cosmology is the standard non-minimal coupling [3, 5, 29]

$$A(\varphi) = \frac{1}{\sqrt{1 + \xi\Phi(\varphi)^2}}, \quad (10)$$

where  $\Phi(\varphi)$  is the scalar field in the physical frame and implicitly given by

$$\varphi = \varphi_0 + \frac{\chi}{2\sqrt{2\xi}} \ln \left[ 1 + 2\chi\Phi \left( \sqrt{1 + \chi^2\Phi^2} + \chi\Phi \right) \right] + \frac{\sqrt{3}}{2} \ln \left[ 1 - 2\sqrt{6\xi}\Phi \frac{\sqrt{1 + \chi^2\Phi^2} - \sqrt{6\xi}\Phi}{1 + \xi\Phi^2} \right], \quad (11)$$

with  $\chi \equiv \sqrt{\xi(1 + 6\xi)}$ , and  $\xi > 0$ . The coupling function of the  $\xi$ -theory,

$$\alpha(\varphi) = -\frac{\sqrt{2\xi}\Phi}{\sqrt{1 + \xi(1 + 6\xi)\Phi^2}}, \quad (12)$$

cannot be written in terms of  $\varphi$  in a closed form, so the calculation has to be done partly in the physical frame with the scalar field described by  $\Phi$ .

The MO theory [4] is an analytical approximation of the  $\xi$ -theory. The function  $A(\varphi)$  has the form

$$A(\varphi) = \left[ \cosh \left( \sqrt{3}\beta(\varphi - \varphi_0) \right) \right]^{\frac{1}{3\beta}}, \quad (13)$$

and the coupling function  $\alpha(\varphi)$  is

$$\alpha(\varphi) = \frac{1}{\sqrt{3}} \tanh \left[ \sqrt{3}\beta(\varphi - \varphi_0) \right]. \quad (14)$$

When  $\beta = -2\xi$ , the three classes of theories in Eqs. (8), (10), and (13) hold some common properties. First, the MO theory can be well approximated by the  $\xi$ -theory. Moreover, the coupling functions in the three classes of theories have the same expansion to the linear order of  $\varphi$ ,

$$\alpha(\varphi) \approx \beta\varphi + O(\varphi^2) \approx -2\xi\varphi + O(\varphi^2), \quad (15)$$

where we have used  $\varphi_0 = 0$ . This means that in the limit of  $\varphi \rightarrow 0$ , behaviors of these theories should be the same.

To show the features of these theories, we plot the coupling function  $\alpha(\varphi)$  in Fig. 1. It is clear that the DEF theory has the strongest coupling, and that the MO theory is a good approximation of the  $\xi$ -theory though the coupling in the MO theory is always a little stronger than that in the  $\xi$ -theory. Especially, the values of  $\alpha(\varphi)$  when  $\varphi \rightarrow \infty$  are different in the  $\xi$  and the MO theories. But they become equal when  $\xi$  goes to infinity.

As show in Refs. [2–4], for suitable choices of  $\beta$ , all these three ST theories can have nonperturbative strong-field deviations from GR, namely the spontaneous scalarization of NSs. This name comes from the analogy to the phenomenon

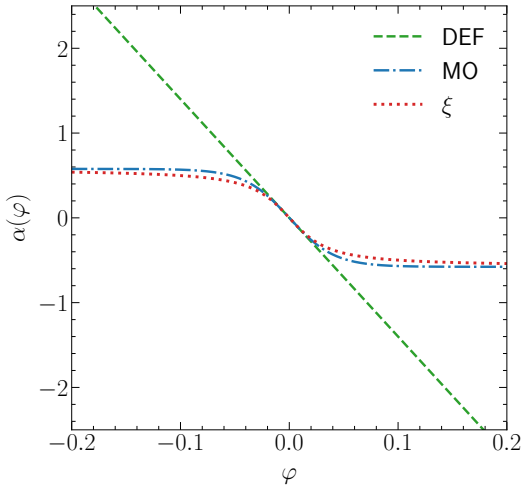


FIG. 1. Coupling function  $\alpha(\varphi)$  for three different theories. We have used  $\beta = -2\xi = -14$ .

of spontaneous magnetization of ferromagnet [3]. The order parameter chosen by Damour and Esposito-Farèse is the scalar charge  $Q$  developed by the NS, which is defined via  $\varphi(r) = \varphi_0 + Q/r + O(r^{-2})$  at  $r \rightarrow \infty$  in the massless DEF theory. This parameter is undefined in massive ST theories due to the exponential Yukawa factor in the asymptotic expansion of the scalar field. But one can take other parameters, for example, the value of the scalar field at the center of the star, as the order parameter and perform the same analysis.

In the absence of the external field  $\varphi_0$ , one can take the star's energy in the form of the usual Landau ansatz near the critical transition point, say,  $\mu(Q) = a(\bar{m}_{\text{cr}} - \bar{m})Q^2/2 + bQ^4/4$ , as a simple model exhibiting spontaneous scalarization, where  $\bar{m}$  is the baryon mass of the star. The energy  $\mu$  is minimal at the trivial solution  $Q = 0$  when  $\bar{m} < \bar{m}_{\text{cr}}$ , while two energetically favored nontrivial solutions appear when  $\bar{m} > \bar{m}_{\text{cr}}$  (cf. the Higgs mechanism in the Standard Model of particle physics). Although  $Q = 0$  is still a solution when  $\bar{m} > \bar{m}_{\text{cr}}$ , it is unstable to any perturbation of the scalar field.

Another way to understand this phenomenon is to consider the instability of the perturbation in the scalar field [24]. To see that, we expand Eqs. (4–5) to the linear order in  $\varphi$ ,

$$R_{\mu\nu} = 8\pi \left( \tilde{T}_{\mu\nu} - \frac{1}{2} g_{\mu\nu} \tilde{T} \right), \quad (16)$$

$$\square\varphi = (m_\varphi^2 - 4\pi\tilde{T}\beta)\varphi. \quad (17)$$

Note that the equation for the metric is irrelevant to the perturbation in the scalar field  $\varphi$ , so we can consider the stability of Eq. (17) in a background metric of the GR solution.

For matters described by a perfect fluid, we have  $\tilde{T} = -\tilde{\epsilon} + 3\tilde{p}$ , which is negative for ordinary matters. So the right hand side in Eq. (17) can be negative for a sufficiently negative  $\beta$  and the scalar field thus suffers an instability (i.e., the tachyonic instability). It also shows that the mass term of the scalar field suppresses the existence of spontaneous scalarization [24]. For highly compact NSs with some EOSs, the condition that  $\tilde{T} < 0$  may not hold in the center of NSs [44].

Therefore, a NS with a large baryonic mass will not have spontaneous scalarization when  $\beta < 0$ . But interestingly, the scalar field may suffer an instability when  $\tilde{T} > 0$  and  $\beta > 0$  [4]. In this work, we only concentrate ourselves on the  $\beta < 0$  case.

### III. NEUTRON STAR STRUCTURES IN MASSIVE SCALAR-TENSOR THEORIES

In this section, we derive NS structures in massive ST theories. Following Refs. [45, 46], we consider a slowly rotating NS. Keeping only the first order of the angular frequency  $\Omega$ , the stationary and axisymmetric metric takes the form

$$\begin{aligned} ds^2 &= g_{\mu\nu} dx^\mu dx^\nu \\ &= -e^{\nu(\rho)} dt^2 + \left(1 - \frac{2m(\rho)}{\rho}\right)^{-1} d\rho^2 + \rho^2 (d\theta^2 + \sin^2\theta d\phi^2) \\ &\quad + 2\rho^2 \sin^2\theta (\omega(\rho, \theta) - \Omega) dt d\phi, \end{aligned} \quad (18)$$

where  $\omega(\rho, \theta)$  is a function at the order of  $\Omega$ . As show by Hartle [45], the function  $\omega(\rho, \theta)$  can be expanded as

$$\omega(\rho, \theta) = \sum_{l=1}^{\infty} \omega_l(\rho) \left( -\frac{1}{\sin\theta} \frac{dP_l}{d\theta} \right), \quad (19)$$

and the radial functions  $\omega_l(\rho)$  satisfy

$$\frac{1}{\rho^4} \frac{d}{d\rho} \left[ \rho^4 j(\rho) \frac{d\omega_l}{d\rho} \right] + \left[ \frac{4}{\rho} - e^{(\lambda-\nu)/2} \frac{l(l+1)-2}{\rho^2} \right] \omega_l = 0, \quad (20)$$

where

$$j(\rho) = e^{-(\nu+\lambda)/2}, \quad (21)$$

$$e^\lambda = \left(1 - \frac{2m(\rho)}{\rho}\right)^{-1}. \quad (22)$$

At large  $\rho$ ,  $\omega_l$  has the form

$$\omega_l \rightarrow \text{const.} \times \rho^{-l-2} + \text{const.} \times \rho^{l-1}. \quad (23)$$

For the space to be flat at large  $\rho$ , the only term remaining is  $l = 1$ , and thus the function  $\omega(\rho, \theta)$  is independent of  $\theta$ .

Substituting Eqs. (6) and (18) into Eqs. (4–5), one obtains systematic differential equations for the metric and the scalar

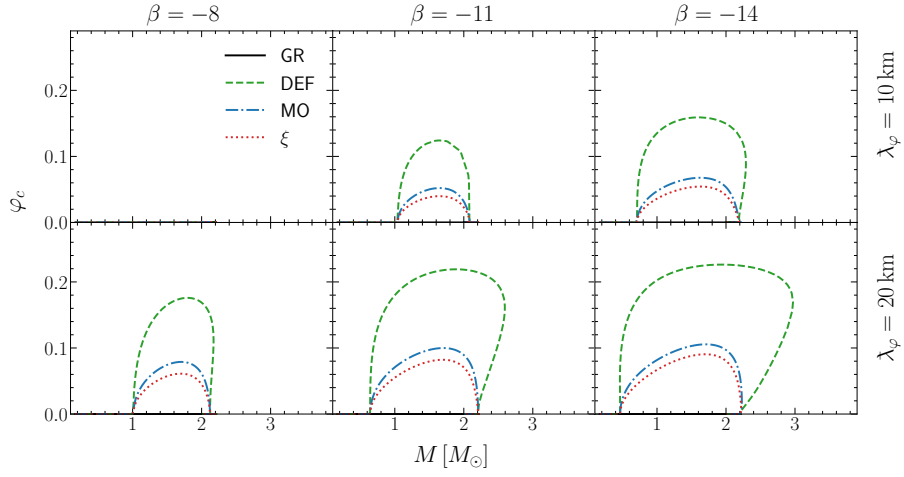


FIG. 2. Spontaneous scalarization in the three theories, where  $\varphi_c$  is the scalar field at the center of the NS and  $M$  is the mass of the NS. EOS AP4 is used in the calculation. For large  $M$ , there are two solutions of  $\varphi_c$ , where the solution with the smaller  $\varphi_c$  is unstable [24]. In the upper left panel, no spontaneous scalarization happens.

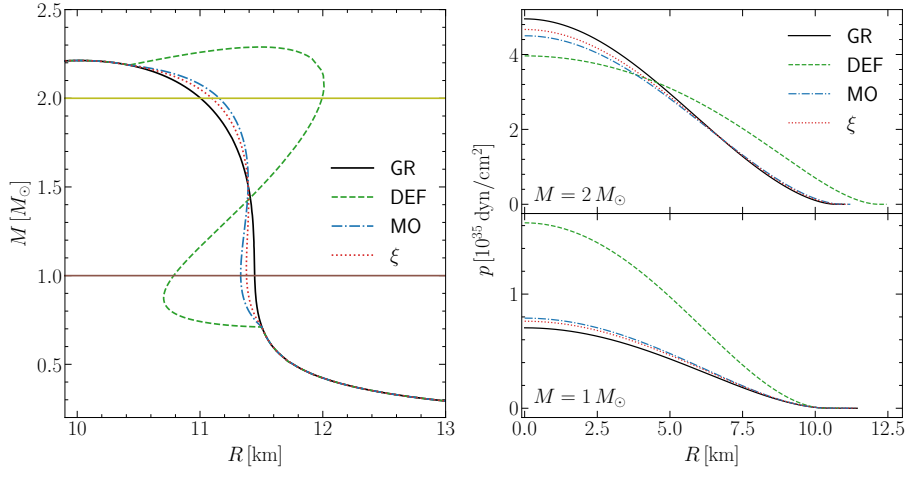


FIG. 3. Mass-radius relation of NSs in GR and the ST theories with  $\beta = -14$  and  $\lambda_\phi = 10$  km (left), and the pressure versus the radius of a NS with  $M = 1 M_\odot$  (lower right) and  $M = 2 M_\odot$  (upper right). EOS AP4 is used in the calculation. The radius  $R$  is defined by  $R = A(\rho)\rho$ , which is the length in the physical frame.

field [1, 3, 24, 29],

$$m' = 4\pi\rho^2 A^4 \tilde{\epsilon} + \frac{1}{2}\rho(\rho - 2m)\varphi'^2 + \frac{1}{4}\rho^2 V, \quad (24)$$

$$v' = \frac{8\pi\rho^2 A^4 \tilde{p}}{\rho - 2m} + \frac{2m}{\rho(\rho - 2m)} + \rho\varphi'^2 - \frac{1}{2}\frac{\rho^2}{(\rho - 2m)}V, \quad (25)$$

$$\begin{aligned} \tilde{p}' = & -(\tilde{\epsilon} + \tilde{p}) \left[ \frac{4\pi\rho^2 A^4 \tilde{p}}{\rho - 2m} + \frac{m}{\rho(\rho - 2m)} \right] \\ & + (\tilde{\epsilon} + \tilde{p}) \left[ \frac{1}{2}\rho\varphi'^2 + \frac{A'}{A} - \frac{1}{4}\frac{\rho^2}{(\rho - 2m)}V \right], \quad (26) \end{aligned}$$

$$\begin{aligned} \varphi'' = & \frac{4\pi\rho A^4}{\rho - 2M} [\rho(\tilde{\epsilon} - \tilde{p})\varphi' + \alpha(\tilde{\epsilon} - 3\tilde{p})] \\ & - \frac{2(\rho - M)}{\rho(\rho - 2M)}\varphi' + \frac{\rho}{\rho - 2M} \left( \frac{1}{2}\rho V\varphi' + \frac{1}{4}\frac{dV}{d\varphi} \right), \quad (27) \end{aligned}$$

$$\omega'' = \frac{4\pi\rho A^4}{\rho - 2m} (\tilde{\epsilon} + \tilde{p})(\rho\omega' + 4\omega) + \left( \rho\varphi'^2 - \frac{4}{\rho} \right) \omega', \quad (28)$$

where the primes denote the derivatives with respect to  $\rho$ .

As mentioned before, for  $\xi$ -theory one needs to calculate with  $\Phi$ , the scalar field in the physical frame. Taking a derivative in Eq. (11), one gets

$$\left( \frac{d\varphi}{d\Phi} \right)^2 = \frac{3}{4} \left( \frac{2\xi\Phi}{1 + \xi\Phi^2} \right)^2 + \frac{1}{2} \frac{1}{1 + \xi\Phi^2}. \quad (29)$$

Using this relation it is easy to change all the  $\varphi'$ ,  $\varphi''$ , and  $d/d\varphi$  appearing in Eqs. (24–28) to  $\Phi'$ ,  $\Phi''$ , and  $d/d\Phi$ ; see Ref. [29] for more details.

To integrate the above equations, we start with the initial values at the center of the NS,

$$\begin{aligned} m(\rho)|_{\rho=0} = 0, \quad v(\rho)|_{\rho=0} = 0, \quad \tilde{p}(\rho)|_{\rho=0} = \tilde{p}_c, \\ \varphi(\rho)|_{\rho=0} = \varphi_c, \quad \varphi'(\rho)|_{\rho=0} = 0, \\ \omega(\rho)|_{\rho=0} = 1, \quad \omega'(\rho)|_{\rho=0} = 0. \quad (30) \end{aligned}$$



Note that the initial value of  $\nu$  is not equal to 0 in the real case, one needs to use the fact that the asymptotic value of  $\nu$  at infinity is 0 to get the real initial value of  $\nu$ . The initial value of  $\omega$  is also given arbitrarily, since the equation for  $\omega$  is homogeneous. Solving Eqs. (24–28) with a given EOS, one gets the structure of a slowly rotating NS in the ST theory. We take AP4 [47] as the example EOS to calculate NS structures in the following.

For suitable choices of the parameters, namely the compactness of the NS and the coupling strength, there exist solutions favouring a non-zero scalar field. In Fig. 2 we show the values of the scalar field at the center of the star versus the Arnowitt-Deser-Misner (ADM) mass of the spacetime for different choices of  $\beta$  and  $\lambda_\varphi$ . The spontaneous scalarization grows with both (the negative value of)  $\beta$  and  $\lambda_\varphi$ . A larger mass of the scalar field can suppress or even prevent the happening of scalarization. Also we find that only those NSs with suitable masses have nontrivial scalar fields. NSs with too small or too large masses only have the GR solution. These features are consistent with the analysis in Sec. II. Namely, as shown in Eq. (17), the scalar field suffers the instability only when  $(m_\varphi^2 - 4\pi\tilde{T}\beta)$  is sufficiently negative, which depends on both the scalar mass and the coupling strength. It is also found that, as expected, when  $\beta = -2\xi$ , the DEF theory has the largest scalar field among these theories. The MO theory has similar behaviours to the  $\xi$ -theory especially for large values of  $|\beta|$ .

Taking  $\beta = -14$  and  $\lambda_\varphi = 10$  km as an example, we plot the mass-radius relation in the left panel of Fig. 3. The results of different theories are qualitatively consistent with expectation. With the appearance of the scalar field, the radius of the star with a small ADM mass becomes smaller and vice versa. One can understand this feature by comparing Eq. (26) with the Tolman-Oppenheimer-Volkoff (TOV) equations in GR,

$$\tilde{p}' = -(\tilde{\epsilon} + \tilde{p}) \left( \frac{4\pi\rho^2\tilde{p}}{\rho - 2m} + \frac{m}{\rho(\rho - 2m)} \right), \quad (31)$$

$$m' = 4\pi\rho^2\tilde{\epsilon}. \quad (32)$$

In Eq. (26), the terms in the right-hand side with the factor  $A^4(\varphi)$  are suppressed by the appearance of the scalar field, which is formally equal to replacing the constant  $G$  by  $A^4(\varphi)G$ . But the scalar field itself provides extra gravitation via the terms in the second line of Eq. (26), as well as extra mass via the second and third terms in the right-hand side of Eq. (24).

For an ordinary NS with spontaneous scalarization, the suppression of  $A^4(\varphi)$  and the extra gravitation provided by the scalar field have the same order of effect inside the NS. As the mass of the NS increases, the suppression effect of  $A^4(\varphi)$  becomes more and more important due to the increase of  $\tilde{p}$  and  $\tilde{\epsilon}$  inside the NS, while the extra gravitation provided by the scalar field changes very slowly when the mass of the NS is not close to the critical transition point of spontaneous scalarization. Thus for a low-mass NS, the appearance of the scalar field makes the radius of the star smaller, while a high-mass NS with spontaneous scalarization has a larger radius. This is illustrated in the left panel of Fig. 3.

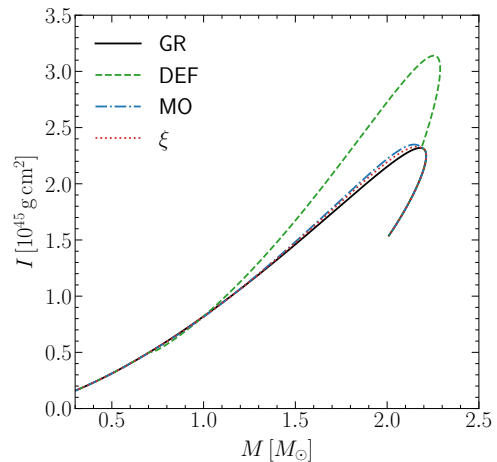


FIG. 4. Moment of inertia  $I$  versus the ADM mass  $M$  with  $\beta = -14$ ,  $\lambda_\varphi = 10$  km. EOS AP4 is used in the calculation.

We also show the pressure  $\tilde{p}$  as a function of  $\rho$  for NSs whose masses are  $M = 1 M_\odot$  and  $M = 2 M_\odot$  respectively in the lower and upper plots in the right panel of Fig. 3. For a low-mass NS with spontaneous scalarization, its  $\tilde{p}$  decreases faster than that in GR due to the extra gravitation caused by the scalar field. For a high-mass NS, the suppression effect of  $A^4(\varphi)$  makes  $\tilde{p}$  change slower.

In Fig. 4 we show the relation between the ADM mass and the moment of inertia  $I$ . The latter is defined by the asymptotic behaviour of the metric element  $g_{t\varphi}$ . When  $\rho \rightarrow \infty$ , we have

$$g_{t\varphi} = (\omega - \Omega)\rho^2 \sin^2 \theta \quad \rightarrow \quad -\frac{2J \sin^2 \theta}{\rho}. \quad (33)$$

Thus the moment of inertia  $I$  can be calculated via

$$I = \frac{J}{\Omega} = \frac{1}{6} \frac{\rho^4 \omega'}{\omega} \Big|_{\rho \rightarrow \infty}. \quad (34)$$

Note that though in the mass-radius relation, a NS with spontaneous scalarization could have a smaller or larger radius than that in GR, the moment of inertia of the NS in the ST theories are almost always larger.

Finally, in Table I we list representative NS parameters in GR and ST theories. One can notice the trend of the increasing scalarization as  $\beta$  and  $m_\varphi$  decrease. Generically speaking, the parameter space for massive ST theories is less constrained than that in the massless case [19–22], in particular that a rather negative  $\beta$  is still allowed by current bounds. Therefore, NSs in massive ST theories can still develop quite different properties from their GR solutions. From the observational aspects, significant changes in the NS radius can be captured by X-ray timing satellite missions like the NICER [35, 36], while significant changes in the NS moment of inertia can be constrained by the Double Pulsar binary system via, say, the Lense-Thirring effect, in the era of the Square Kilometre Array (SKA) [31]. The DEF theory has particularly large effects to be probed.

TABLE I. NS structures in GR and the ST theories with EOS AP4.

Theory	GR	$\beta = -11, \lambda_\varphi = 10 \text{ km}$			$\beta = -14, \lambda_\varphi = 10 \text{ km}$			$\beta = -11, \lambda_\varphi = 20 \text{ km}$			$\beta = -14, \lambda_\varphi = 20 \text{ km}$			
		DEF	MO	$\xi$	DEF	MO	$\xi$	DEF	MO	$\xi$	DEF	MO	$\xi$	
$M = 1 M_\odot$	$\varphi_c$	0	0	0	0	0.135	0.047	0.036	0.180	0.071	0.055	0.203	0.082	0.067
	$R [\text{km}]$	11.4	11.4	11.4	11.4	10.8	11.3	11.4	10.7	11.3	11.3	10.6	11.2	11.3
	$I [10^{45} \text{ g cm}^2]$	0.82	0.82	0.82	0.82	0.82	0.82	0.82	0.86	0.82	0.82	0.95	0.82	0.82
$M = 2 M_\odot$	$\varphi_c$	0	0.099	0.032	0.023	0.149	0.053	0.041	0.219	0.089	0.071	0.226	0.097	0.080
	$R [\text{km}]$	11.0	11.4	11.1	11.0	12.0	11.2	11.1	12.5	11.3	11.2	12.9	11.4	11.3
	$I [10^{45} \text{ g cm}^2]$	2.15	2.35	2.17	2.16	2.73	2.22	2.19	3.18	2.29	2.24	3.70	2.33	2.27

#### IV. X-RAY PULSAR PULSE PROFILES

We will discuss the X-ray pulsar pulse profiles in detail in this section. As an important goal of the hard X-ray timing instrument (e.g., NICER), using the pulse profile observations from the hot spots on NS surfaces could help people to measure the masses and radii of NSs to an accuracy of a few percents [35, 36, 48], which can be used to determinate the EOS of the NSs. As show in Fig. 3, for a given EOS, the mass-radius relation for scalarized NSs can have a large deviation from that in GR. Consequently, The mass-radius relation of NSs can also be used to constrain the parameter space of massive ST theories. In the meanwhile, the appearance of the scalar field also affects the pulse profiles. In this section, we follow Refs. [29, 33] and calculate the pulse profiles from a pair of extended hot spots on the surface of a NS with spontaneous scalarization.

Following the assumptions in Refs. [49, 50], we consider a model with a pair of hot spots sitting oppositely on the surface of a slowly rotating NS. For simplicity, the metric outside the NS is taken to be spherically symmetric. We neglect the effects of rotation and the deformations of the NS on the spacetime, which have been shown to be small in GR for a slowly rotating NS [33]. We also assume that the distance between the NS and the observer is large enough so that it can be treated mathematically as infinity.

The geodesic equation for photons holds in the physical frame, so we need to use the physical metric  $\tilde{g}_{\mu\nu} = A^2(\varphi)g_{\mu\nu}$  to compute photon trajectories. We define a new radial coordinate  $r = A(\varphi)\rho$ , and the metric outside the star can be written as

$$d\tilde{s}^2 = -g(r)dt^2 + f(r)dr^2 + r^2 d\theta^2 + r^2 \sin^2 \theta d\phi^2, \quad (35)$$

with the coefficients

$$f = \left(\frac{d\rho}{dr}\right)^2 A^2 \left(1 - \frac{2m(\rho)}{\rho}\right)^{-1}, \quad g = A^2 e^\nu. \quad (36)$$

As shown in Ref. [29], for a point-like hot spot, the observed flux can be expressed as

$$F(\nu) = g(R)\delta^4 I'(\nu', \alpha') \frac{\sin \alpha \cos \alpha}{\sin \psi} \frac{d\alpha}{d\psi} \frac{dS'}{D^2}, \quad (37)$$

where  $R$  is the radius of the star,  $\delta$  is the Doppler factor caused by the rotation,  $I'(\nu', \alpha')$  is the radiation intensity at emission,  $\alpha$  represents the emission angle of the photons with respect to the local radial direction,  $dS'$  is the proper differential area where the photons are emitted,  $D$  is the distance to the star and all primed quantities are measured in the local rest frame on the surface of the NS (see Fig. 8 in Ref. [29] for illustration).

If photons emitted at an angle  $\alpha$  eventually propagate along the line of sight and thus are observed, the angle  $\psi$ , spanning from the local radial direction to the line of sight, must be related to the emission angle  $\alpha$  via

$$\psi = \sigma \int_R^\infty \frac{fg}{r^2} \frac{1}{\sqrt{1 - \sigma^2 g/r^2}} dr, \quad (38)$$

where  $\sigma \equiv R \sin \alpha / \sqrt{g(R)}$  is the impact parameter.

The relative time delay can be defined by

$$\begin{aligned} \delta t &= t - t_0 - \int_R^\infty \sqrt{\frac{f}{g}} dr \\ &= \int_R^\infty \sqrt{\frac{f}{g}} \left( \frac{1}{\sqrt{1 - \sigma^2 g/r^2}} - 1 \right) dr, \end{aligned} \quad (39)$$

where  $t$  is the observation time and  $t_0$  is the emission time.

To consider a more realistic model, we extend the point-like hot spots in Refs. [29, 33] to finite regions. Following the method in Ref. [50], we put a grid of emission spots across the stellar surface to construct X-ray emission regions and keep the radiation intensity the same as the point-like spots. Then, using geometric relations one can calculate the observed angle  $\psi$  in terms of the location of the observer, the locations of the hot spots, and the star's rotating phase. The observation time is related to  $\psi$  by Eq. (39). For each infinitesimal hot spot one calculates the flux by Eq. (37) and sums them up to get the total flux received at a certain observation time.

From the mass-radius relation shown in Fig. 3, we find that the scalarized NSs have the largest deviation from GR in the radii around  $M = 1.0 M_\odot$  and  $M = 2.0 M_\odot$ . Thus in Fig. 5, we plot the X-ray pulsar profiles for two NSs with ADM masses  $M = 1.0 M_\odot$  (upper set of curves) and  $M = 2.0 M_\odot$  (lower set of curves). We take the angle between the NS spin axis and the hot spots to be  $\pi/6$  and the spin axis is at an angle  $\pi/3$  to the observer. The left column in this figure is for the model

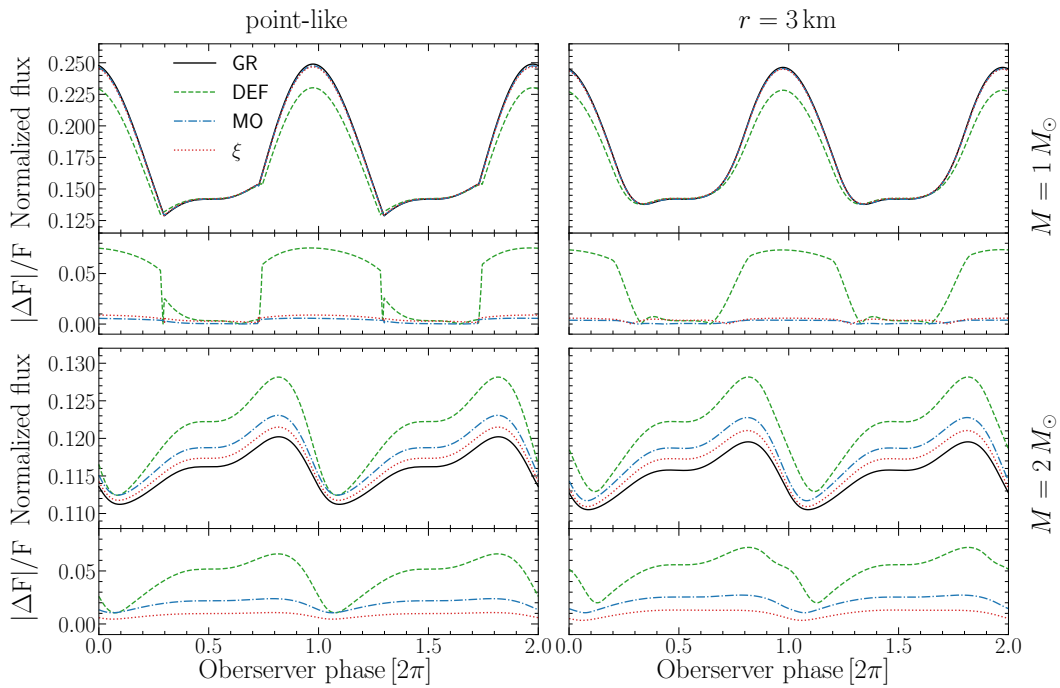


FIG. 5. X-ray pulse profiles for NSs with isotropic emission intensity  $I$ . The left column is the results from point-like hot spots while the right column is the results from extended hot spots with spherical radius  $r = 3$  km. The masses of the NSs are chosen as  $1 M_{\odot}$  for the upper set of curves and  $2 M_{\odot}$  for the lower set of curves. The percental deviations from GR are plotted. The integral radiating intensities of hot spots on the surface of NSs are chosen to be the same for the two cases. The angle between the NS spin axis and the hot spot on the northern hemisphere is  $\pi/6$  and the spin axis is at an angle  $\pi/3$  with respect to the line of sight. The rotating frequency  $f$  of the pulsar is assumed to be 250 Hz. We have used EOS AP4 in the calculation.

TABLE II. X-ray pulse profiles for NSs in GR and the ST theories. Results are only shown for the model with the isotropic radiation intensity and point-like hot spots. We have used EOS AP4 in the calculation.

Theory	GR	$\beta = -11, \lambda_{\varphi} = 10$ km				$\beta = -14, \lambda_{\varphi} = 10$ km				$\beta = -11, \lambda_{\varphi} = 20$ km				$\beta = -14, \lambda_{\varphi} = 20$ km			
		DEF	MO	$\xi$	DEF	MO	$\xi$	DEF	MO	$\xi$	DEF	MO	$\xi$	DEF	MO	$\xi$	
$M = 1 M_{\odot}$	peak flux	0.249	0.249	0.249	0.249	0.230	0.248	0.247	0.219	0.244	0.246	0.202	0.241	0.242			
	flux deviation (%)	0	0.000	0.000	0.000	7.53	0.569	0.891	12.2	1.84	1.36	19.0	3.23	2.63			
	peak phase ( $2\pi$ )	0.976	0.976	0.976	0.976	0.976	0.976	0.976	0.976	0.976	0.976	0.974	0.976	0.976			
	phase deviation (%)	0	0.00	0.00	0.00	0.00	0.00	0.00	0.00	0.00	0.00	0.18	0.00	0.00			
$M = 2 M_{\odot}$	peak flux	0.120	0.125	0.122	0.120	0.128	0.123	0.121	0.126	0.124	0.122	0.121	0.125	0.124			
	flux deviation (%)	0	4.67	1.70	0.309	7.03	2.78	1.47	5.14	3.29	2.28	1.30	4.19	3.30			
	peak phase ( $2\pi$ )	0.820	0.814	0.816	0.820	0.818	0.816	0.818	0.818	0.814	0.816	0.823	0.813	0.814			
	phase deviation (%)	0	0.64	0.43	0.00	0.21	0.43	0.21	0.21	0.64	0.43	0.43	0.85	0.64			

with point-like hot spots and the right column is for the model with extended circular emission regions of 3 km radius.

One can notice that for NSs with spontaneous scalarization, the phases of the profiles are almost the same as that in GR, which means that the time delay of the photons in the ST theories is almost the same as that in GR. It is reasonable because the scalar field suffers an exponential suppression with a characteristic length of  $\lambda_{\varphi}$  outside the star and the metric quickly becomes equal to that of GR. In the numerical results shown in Fig. 5, the length  $\lambda_{\varphi}$  is chosen to be 10 km, which is

about the same as the NS's radius. The region with remarkable values of the scalar field is only inside the NS. The main difference of the X-ray profiles in Fig. 5 is the amplitudes of the fluxes, which have noticeable deviations from GR around the peaks of the profiles. This feature is mainly related to the difference in the mass-radius relation and dominated by the gravitational redshift. According to Fig. 5, the difference between the point-like model and the extended model is relatively small. Therefore, for a hot spot with radius about 3 km, the point-like model is a good approximation.



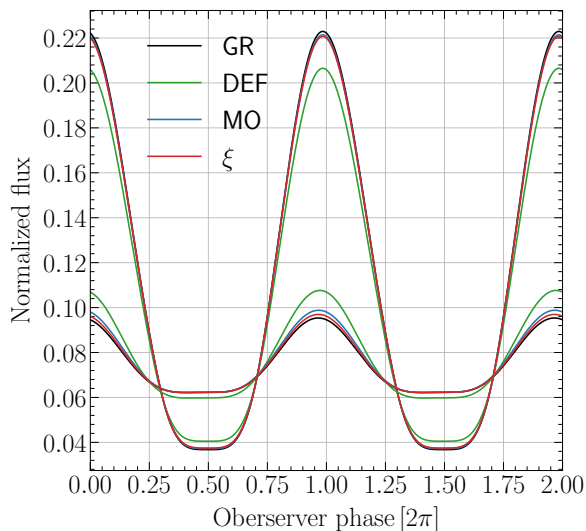


FIG. 6. X-ray pulse profiles for NSs with anisotropic emission intensity  $I'$ . Here the curves are results from point-like hot spots. The masses of the NSs are chosen as  $1 M_{\odot}$  for the upper set of curves and  $2 M_{\odot}$  for the lower set of curves. The integral radiating intensities of hot spots on the surface of NSs are chosen to be the same. Other parameters are the same as in Fig. 5. We have used EOS AP4 in the calculation.

In the above discussion, the specific intensity of the radiation of the two hot spots is assumed to be isotropic. This assumption holds if the two hot spots are blackbodies and sit in vacuum. However, for realistic NSs, the presence of magnetic fields and Compton scattering can result in the “limb-darkening” effect so that the radiation intensity decreases with the angle  $\alpha'$  [49, 51]. This effect can change the features of the profiles significantly. To our best knowledge, this effect is considered numerically in ST theories for the first time in this work.

For numerical study of the limb-darkening effect, we take a simple form of the intensity

$$I'(v', \alpha') = \cos \alpha'. \quad (40)$$

In Fig. 6 we show the X-ray profiles for the two NSs with the same parameters as in Fig. 5 but with the anisotropic specific intensity. One can notice that the limb-darkening effect partly reduces the effect of beaming and gives a much smoother curve. For NSs with spontaneous scalarization, the main deviations from GR still occur at the peak of the profiles.

To give a quantitative description of the differences in the X-ray profiles between GR and the ST theories, we present some numerical results in Table II. In the table, we show the peak values of the normalized fluxes and the related observer phases for different choices of parameters. One can see that the deviations are mainly in the peak fluxes of the profiles, which can be about 10% for the DEF theory and about 2% for the  $\xi$  and the MO theories. The deviations in phase are generally small, and can actually only be seen in the case of  $M = 2 M_{\odot}$ . The deviations for the DEF theory are much larger than those of the  $\xi$  and the MO theories, which is consistent

with the size of scalarization shown in Fig. 2. One may notice that for the last column of the DEF theory, the peak fluxes and the deviations are smaller than those of the MO and the  $\xi$  theory. This is because the DEF theory has strong scalarization so the radius of the NS is larger compared to the other two theories, and in this case, the radius is too large so that the flux from one of the hot spots is blocked by the star itself when the total flux reaches the peak. For the MO or the  $\xi$  theories, the scalarization is weaker than the DEF theory and the radius of the NS of the same mass is smaller. The fluxes from both of the hot spots can be received by the observer when the total flux reaches the peak.

## V. TIDAL LOVE NUMBERS IN THE ST THEORIES

GW observation of binary NS mergers provides unique possibilities to study the EOS of the NS and to test GR [38, 52]. At the early stage of the inspiral, the evolution of the system is dominated by the point-mass dynamics. But as the system evolves to the end of the inspiral, the finite-size effect starts to show its influence on the GW signal. Phenomena like tidal effects which depend on the EOS of the NS can lead to a small change of the waveform’s phasing behaviour. Thanks to the matched filtering technique used in the signal analysis, high sensitivities to the phase evolution in GWs can be achieved, therefore leading to measurements of tidal effects. The well-known GW discovery of GW170817 has been used to constrain the tidal deformability parameter for the first time [13, 39].

NSs’ tidal deformability is defined as the ratio of the induced tidal deformation to the strength of the tidal perturbation [38]. In GR, the metric coefficient  $g_{tt}$  of a tidally deformed NS can be expanded as

$$-\frac{1 + g_{tt}}{2} = -\frac{M}{\rho} - \frac{3Q_{ij}}{2\rho^3}(n^i n^j - \frac{1}{3}\delta^{ij}) + O\left(\frac{1}{\rho^4}\right) + \frac{1}{2}\mathcal{E}_{ij}x^i x^j + O(\rho^3), \quad (41)$$

in the star’s local asymptotic rest frame [38], where  $M$  is the star’s mass,  $Q_{ij}$  is the induced quadrupole moment,  $\mathcal{E}_{ij}$  is the external tidal field, and  $n^i \equiv x^i/\rho$ . To the linear order in  $\mathcal{E}_{ij}$ , the induced quadrupole will have the form  $Q_{ij} = -\lambda\mathcal{E}_{ij}$ . Here, the parameter  $\lambda$  represents the tidal deformability of the star, which is related to the  $l = 2$  tidal Love number  $k_2$  via  $k_2 = 3G\lambda R^5/2$ .

Considering ST theories, we need to expand the metric with the possible perturbations in the scalar field. For the massive scalar field, the asymptotic behavior of the scalar field and its perturbation have the form

$$\varphi \text{ and } \delta\varphi \rightarrow \frac{1}{\rho}e^{-\rho/\lambda_{\varphi}}. \quad (42)$$

Such an exponential drop will not affect the expansion (41) in any order of  $1/\rho$ , which is different from the massless case [40]. Even though the scalar field perturbation is

Yukawa-suppressed, the scalarized NS itself will respond differently to a tidal field, which leads to a different tidal deformability.

Restricting to the  $l = 2$ , static, even-parity perturbations in the Regge-Wheeler gauge [53], the perturbations in the metric and the scalar field can be written as

$$\delta g_{\mu\nu}^{(2m)} = Y_{2m}(\theta, \phi) \begin{bmatrix} -e^\nu H_0 & H_1 & 0 & 0 \\ H_1 & H_2 / \left(1 - \frac{2m}{\rho}\right) & 0 & 0 \\ 0 & 0 & \rho^2 K & 0 \\ 0 & 0 & 0 & \rho^2 \sin^2 \theta K \end{bmatrix}, \quad (43)$$

$$\delta\varphi^{(2m)} = Y_{2m}(\theta, \phi) \delta\varphi, \quad (44)$$

where  $H_0, H_1, H_2, K$  and  $\delta\varphi$  are functions only depending on  $\rho$ , and  $Y_{lm}$  are the spherical harmonics.

Following the procedure in the original work by Hinderer [38], we combine Eqs. (43–44) with the linearized Einstein equations,  $\delta G_\nu^\mu = 8\pi\delta T_\nu^\mu$ , and get

$$H_1 = 0, \quad (45)$$

$$H_0 = -H_2 = H(\rho), \quad (46)$$

$$K = \int [-H'(\rho) - H(\rho)v'(\rho) - 4\delta\varphi(\rho)\varphi(\rho)] dr. \quad (47)$$

Together with the linearized perturbation of Eq. (5), one finally gets the differential equations for  $H$  and  $\delta\varphi$ ,

$$H'' + c_1 H' + c_0 H = c_s \delta\varphi, \quad (48)$$

$$\delta\varphi'' + d_1 \delta\varphi' + d_0 \delta\varphi = d_s H, \quad (49)$$

where

$$c_1 = d_1 = \frac{4 - 2x - \rho^2 V + 8\pi\rho^2 A^4(\tilde{p} - \tilde{\epsilon})}{2\rho(1-x)}, \quad (50)$$

$$c_s = 4d_s = \frac{1}{1-x} \left\{ 8\pi A^4 \alpha \left[ \tilde{\epsilon} \left(1 - \frac{d\tilde{\epsilon}}{d\tilde{p}}\right) + \tilde{p} \left(9 - \frac{d\tilde{\epsilon}}{d\tilde{p}}\right) \right] + 32\pi\rho A^4 \tilde{p}\varphi' - \frac{dV}{d\varphi} - 2\rho\varphi' \left[ V - 2\varphi'^2 + 2x \left(\varphi'^2 - \frac{1}{\rho^2}\right) \right] \right\}, \quad (51)$$

$$c_0 = \frac{4\pi A^4(\tilde{p} + \tilde{\epsilon})}{1-x} \frac{d\tilde{\epsilon}}{d\tilde{p}} - \frac{1}{(1-x)^2} \left\{ \frac{x^2}{\rho^2} (\rho^2 \varphi'^2 - 1)^2 - x \left[ \frac{6}{\rho^2} - 2\varphi'^2 + 2\rho^2 \varphi'^4 + V(2 - \rho^2 \varphi'^2) + 4\pi A^4 (\tilde{p} [4\rho^2 \varphi'^2 - 13] - 5\tilde{\epsilon}) \right] \right. \\ \left. + 64\pi^2 \rho^2 A^8 \tilde{p}^2 + \frac{\rho^2 V^2}{4} + \frac{6}{\rho^2} + \rho^2 \varphi'^4 + V(1 - \rho^2 \varphi'^2) - 4\pi A^4 [5\tilde{\epsilon} + \tilde{p}(9 + 2\rho^2 V - 4\rho^2 \varphi'^2)] \right\}, \quad (52)$$

$$d_0 = \frac{4}{1-x} \left\{ \pi A^4 \alpha^2 (\tilde{p} + \tilde{\epsilon}) \frac{d\tilde{\epsilon}}{d\tilde{p}} + \left[ 6\pi A^4 \alpha^2 (\tilde{p} - \tilde{\epsilon}) - (1-x)\varphi'^2 - \frac{3}{2\rho^2} \right] + \pi\rho^2 A^3 (3\tilde{p} - \tilde{\epsilon}) A'' - \frac{1}{16} V'' \right\}, \quad (53)$$

where  $x \equiv 2m/\rho$ .

Note that Eqs. (48–49) are linear equations of  $H$  and  $\delta\varphi$ . To solve them, one can integrate the system twice with the initial values [40]

$$H|_{R_0} = R_0^2, \quad H'|_{R_0} = 2R_0, \quad \delta\varphi|_{R_0} = 0, \quad \delta\varphi'|_{R_0} = 0, \quad (54)$$

and

$$H|_{R_0} = 0, \quad H'|_{R_0} = 0, \quad \delta\varphi|_{R_0} = R_0^2, \quad \delta\varphi'|_{R_0} = 2R_0, \quad (55)$$

respectively, where  $R_0$  is a small radius. Then one needs to make a linear combination of these two results to construct a solution whose asymptotic value of  $\delta\varphi$  vanishes.

For a massive scalar field, the asymptotic form of the metric is the same as that in GR. So one can integrate the system to a sufficiently large  $\rho = \rho_i$  and ignore the scalar field for  $\rho > \rho_i$ . Define

$$C = \frac{m}{\rho} \Big|_{\rho \rightarrow \rho_i}, \quad y = \frac{\rho H'}{H} \Big|_{\rho \rightarrow \rho_i}, \quad (56)$$

and then the tidal deformability can be calculated by [38]

$$\lambda = \frac{2}{3} \rho_i^5 \frac{8C^5}{5} (1 - 2C)^2 [2 + 2C(y - 1) - y] \\ \times \left\{ 4C^3 [13 - 11y + C(3y - 2) + 2C^2(1 + y)] \right. \\ \left. + 3(1 - 2C)^2 [2 - y + 2C(y - 1)] \ln(1 - 2C) \right. \\ \left. + 2C [6 - 3y + 3C(5y - 8)] \right\}^{-1}. \quad (57)$$

The case is different for a massless scalar field, as can be seen in Ref. [40]. The nonzero scalar charge developed by the scalar field will affect  $\lambda$  and make it different in the Einstein and physical frame; see Eq. (B8) in Ref. [40].

In Fig. 7, we show the relation between the tidal deformability  $\lambda$  and the NS's ADM mass  $M$  for the ST theories and GR. The parameters for the ST theories are the same as those in Fig. 2. Since the tidal deformability is proportional to  $R^5$ , the deviations of the tidal deformability follow the trend of, but are qualitatively larger than, the mass-radius relation shown in Fig. 3.

From Fig. 7 we can see that the largest deviation happens around  $M = 1 M_\odot$  and  $M = 2 M_\odot$ , so we list the deviations of the tidal deformability in the ST theories with  $M = 1 M_\odot$

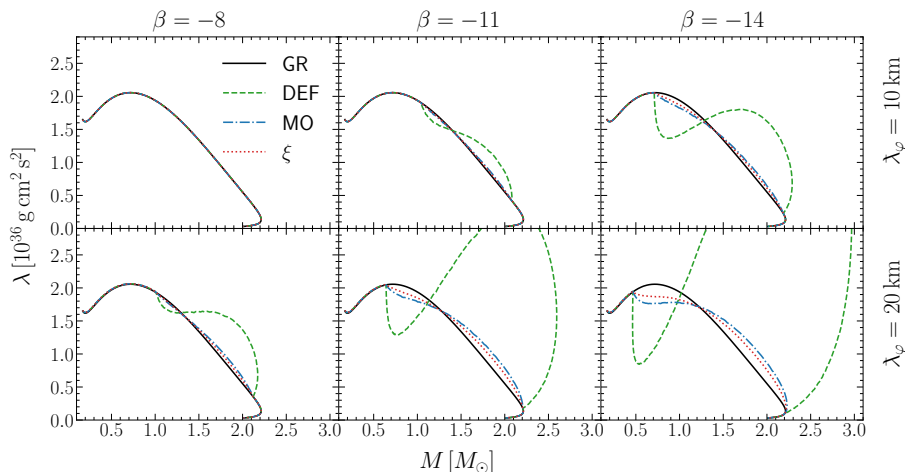


FIG. 7. The tidal deformability  $\lambda$  versus the ADM mass  $M$  in different ST theories with EOS AP4.

TABLE III. Tidal deformabilities and their percentage deviations from GR in the ST theories with  $M = 1 M_\odot$  and  $M = 2 M_\odot$ . We have used EOS AP4 in the calculation.

Theory	GR	$\beta = -11, \lambda_\varphi = 10 \text{ km}$			$\beta = -14, \lambda_\varphi = 10 \text{ km}$			$\beta = -11, \lambda_\varphi = 20 \text{ km}$			$\beta = -14, \lambda_\varphi = 20 \text{ km}$			
		DEF	MO	$\xi$	DEF	MO	$\xi$	DEF	MO	$\xi$	DEF	MO	$\xi$	
$M = 1 M_\odot$	$\lambda [10^{36} \text{ g cm}^2 \text{ s}^2]$	1.94	1.94	1.94	1.41	1.82	1.87	1.57	1.79	1.85	1.85	1.78	1.82	
	deviation (%)	0	0.00	0.00	27.0	5.97	3.58	19.1	7.59	4.64	4.37	8.26	6.09	
$M = 2 M_\odot$	$\lambda [10^{36} \text{ g cm}^2 \text{ s}^2]$	0.551	0.857	0.578	0.567	1.62	0.644	0.609	3.17	0.786	0.693	5.29	0.865	0.757
	deviation (%)	0	55.5	4.90	2.92	194	16.8	10.5	475	42.6	25.7	860	56.9	37.3

and  $M = 2 M_\odot$  in Table III. The deviations increase quickly with  $|\beta|$  and  $\lambda_\varphi$ . The scalarized NS with  $M = 2 M_\odot$  in the DEF theory can have a tidal deformability almost 10 times greater than that in GR, thus providing an important window for tests.

## VI. UNIVERSAL RELATION IN MASSIVE SCALAR-TENSOR THEORIES

The dimensionless moment of inertia  $\bar{I} = I/M^3$  and the dimensionless tidal Love number  $\bar{\lambda} = \lambda/M^5$  satisfy a remarkable universal relation in GR [41, 42]. This relation is not affected by the NS EOS up to an accuracy of a few percents. It will allow people to test GR without knowing the details of the NS EOS, if the universal relations in ST theories are sufficiently different from those in GR. Pani and Berti [40] have calculated the slowly rotating and tidally deformed NSs in the massless DEF theory. They find that the  $\bar{I}$ - $\bar{\lambda}$ - $\bar{Q}$  relations agree with GR in a high accuracy for the allowed parameter space  $\beta > -4.5$ , which is set by the timing data of the pulsar-white dwarf systems [19–22]. But the deviation can reach to nearly 10% for some parameters that are already ruled out. Doneva *et al.* [55] calculated the  $\bar{I}$ - $\bar{Q}$  in the massless DEF theory for rapidly rotating NSs with  $\beta = -4.5$ . The universal relation between  $\bar{I}$  and  $\bar{Q}$  still holds and the deviations from GR are small and hard to test with future astrophysical observations.

Due to the Yukawa suppression originated from the mass

term, massive ST theories can avoid most of the constraints of previous observations. Thus one might expect considerable deviations from GR in the universal relations in certain yet-allowed parameter space. Doneva and Yazadjiev [56] constructed the model of rapidly rotating NSs in the massive DEF theory. They find that the  $\bar{I}$ - $\bar{Q}$  universal relation is nearly EOS independent and the deviations from GR can be large for some allowed parameters.

In Fig. 8 we plot the  $\bar{I}$ - $\bar{\lambda}$  universal relation for the massive ST theories with different choices of parameters. Panels in the first and third rows are the  $\bar{I}$ - $\bar{\lambda}$  relation for EOSs AP4 [47], WFF1 [57], and SLy4 [58]. Panels in the second and fourth rows are the relative deviations from the fitted curve, which is the GR result given in Ref. [54]. From the figure we can see that the  $\bar{I}$ - $\bar{\lambda}$  universal relation still holds in the massive ST theories to a rather good precision. For the MO theory and the  $\xi$ -theory, the largest deviation from GR is within only a few percents. Though the deviations increase with  $|\beta|$  and  $\lambda_\varphi$ , there exist upper limits for the coupling function in these two theories as shown in Fig. 1, and thus the deviations in the  $\bar{I}$ - $\bar{\lambda}$  relation also stay finite and not too large. Differently for the DEF theory, the coupling function shown in Fig. 1 is unbound as  $\varphi$  increases, so the deviation in the  $\bar{I}$ - $\bar{\lambda}$  relation can be as large as 10% in Fig. 8. Comparably significant deviations in the  $\bar{I}$ - $\bar{\lambda}$  relation as the scalarization becomes strong were also observed in the massless DEF theory in Ref. [40].

We mention that there is also a universal relation between

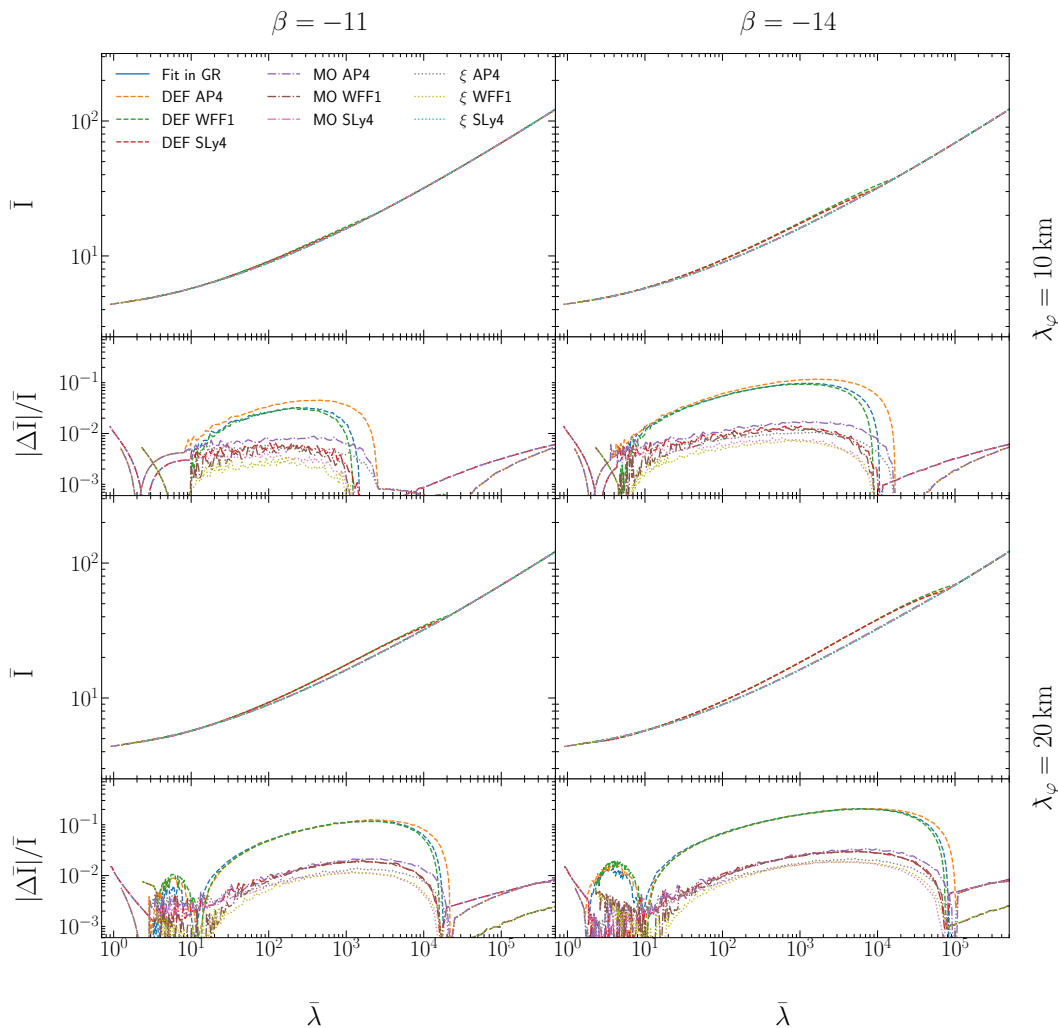


FIG. 8.  $\bar{I}$ - $\bar{\lambda}$  universal relation for three ST theories with different  $\beta$  and  $\lambda_\varphi$ . We consider their EOSs, i.e., AP4, WFF1, and SLy4. The fitted curve for GR is taken from Ref. [54].

the dimensionless moment of inertia  $\bar{I}$  and the star's compactness  $C = M/R$  in both GR [59] and scalar tensor theories [60], as show in Fig. 9. We show the relation in three ST theories with EOSs AP4, WFF1, and SLy4 for  $\beta = -14$  and  $\lambda_\varphi = 10$  km. The fitted curve in GR is derived with a fifth polynomial fitting. The relation between the moment of inertia and the star's compactness seems to have larger dependence on the EOS than the  $\bar{I}$ - $\bar{\lambda}$  universal relation.

## VII. SUMMARY

In this work, we study the NS structures in the DEF, the MO and the  $\xi$  theories with a massive scalar field. The coupling functions to matters differ in these theories. Our investigation serves complementary studies to the massless case. Differential equations for a slowly rotating NS are derived and solved numerically. We analyze and compare the mass-radius relation and the moment of inertia of scalarized

NSs in those theories in detail, pertaining to experiments like NICER [35, 36, 48] and SKA [31]. The structures of the scalarized NSs in those theories have qualitatively similar behaviours, except that the DEF theory, with a linear coupling function, has much larger scalarization compared to the MO and the  $\xi$  theories whose coupling functions are bounded (see Fig. 1). Compared to the massless case, a massive scalar field results in Yukawa suppression which in general introduces smaller deviations from GR and thus can avoid current experimental constraints more easily.

As an application of the numerical results of the NS solutions, we calculate the X-ray profiles from a pair of hot spots on the surfaces of scalarized NSs. We consider a slowly rotating NS but neglect the frame-dragging effect in the metric which is minute here anyway. By taking a model of extended hot spots, which is done for the first time in ST theories, we show that for finite circular hot spots with 1 km radius, the simple model of point-like hot spots is still a good approximation. Deviations from GR mainly happen at the peaks of the profiles. For the DEF theory, the flux deviations can ex-

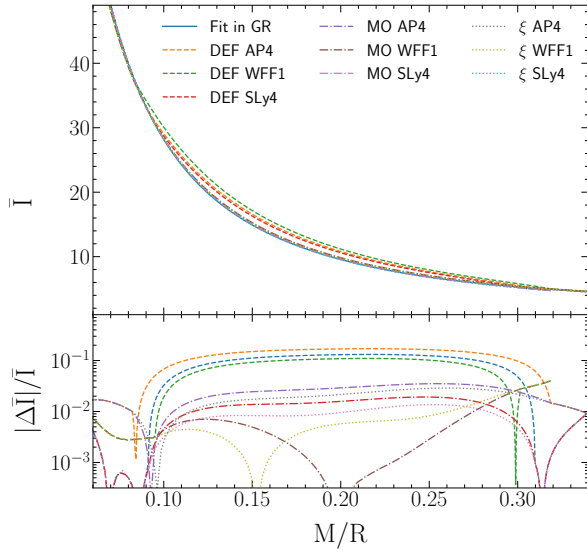


FIG. 9. The universal relation between  $\bar{I}$  and  $M/R$  for three ST theories with  $\beta = -14$  and  $\lambda_\phi = 10$  km. The fitted curve is derived via a fifth polynomial fitting for GR with EOSs AP4, WFF1, and SLy4.

ceed 10% while for the MO and the  $\xi$  theories, this number is about 3%. The phase deviations in the three ST theories are all within 1% which means that it is hard to test with observations from pulsar timing. We also study the limb-darkening effect and show that it can smooth the pulse profiles but not much affect the level of deviations from GR. These studies will provide useful inputs to X-ray timing missions like NICER in

testing alternative gravity theories.

In addition, for the first time we calculate the tidal deformability of NSs in the massive ST theories. The results are qualitatively consistent with the massless case, but due to the mass term of the scalar field, massive ST theories have much larger yet-allowed parameter space unconstrained where large deviations from GR are possible. We investigate the  $\bar{I}$ - $\bar{\lambda}$  universal relation in the massive ST theories. For the MO and the  $\xi$  theories, the deviations from GR are within a few percents due to their finite coupling functions; but for the DEF theory, the deviation can exceed 10% and be even higher for sufficiently large  $|\beta|$  and  $|\lambda_\phi|$ . It will be interesting to test the massive ST theories with the universal relation via the observations of binary NS mergers and their associated GWs.

## ACKNOWLEDGMENTS

We are grateful to Norbert Wex for carefully reading the manuscript and providing helpful comments, and the anonymous referee for constructive suggestions. This work was supported by the National SKA Program of China (2020SKA0120300), the National Natural Science Foundation of China (11975027, 11991053, 11721303), the Young Elite Scientists Sponsorship Program by the China Association for Science and Technology (2018QNRC001), the Max Planck Partner Group Program funded by the Max Planck Society, and the High-performance Computing Platform of Peking University. ZH is supported by the Principal's Fund for the Undergraduate Student Research Study at Peking University, and RX is supported by the Boya Postdoctoral Fellowship at Peking University.

- 
- [1] T. Damour and G. Esposito-Farèse, *Class. Quant. Grav.* **9**, 2093 (1992).
- [2] T. Damour and G. Esposito-Farèse, *Phys. Rev. Lett.* **70**, 2220 (1993).
- [3] T. Damour and G. Esposito-Farèse, *Phys. Rev. D* **54**, 1474 (1996).
- [4] R. F. Mendes and N. Ortiz, *Phys. Rev. D* **93**, 124035 (2016).
- [5] A. Savaş Arapoğlu, K. Y. Ekşi, and A. Emrah Yükselci, *Phys. Rev. D* **99**, 064055 (2019).
- [6] C. M. Will, *Theory and Experiment in Gravitational Physics* (Cambridge University Press, Cambridge, England, 2018).
- [7] P. C. C. Freire, N. Wex, G. Esposito-Farèse, J. P. W. Verbiest, M. Bailes, B. A. Jacoby, M. Kramer, I. H. Stairs, J. Antoniadis, and G. H. Janssen, *Mon. Not. Roy. Astron. Soc.* **423**, 3328 (2012), arXiv:1205.1450 [astro-ph.GA].
- [8] L. Shao and N. Wex, *Sci. China Phys. Mech. Astron.* **59**, 699501 (2016), arXiv:1604.03662 [gr-qc].
- [9] L. Shao, *AIP Conf. Proc.* **2127**, 020016 (2019), arXiv:1901.07546 [gr-qc].
- [10] K. Liu *et al.*, *Mon. Not. Roy. Astron. Soc.* **499**, 2276 (2020), arXiv:2009.12544 [astro-ph.HE].
- [11] G. Esposito-Farèse, *AIP Conf. Proc.* **736**, 35 (2004), arXiv:gr-qc/0409081 [gr-qc].
- [12] N. Sennett, L. Shao, and J. Steinhoff, *Phys. Rev. D* **96**, 084019 (2017), arXiv:1708.08285 [gr-qc].
- [13] B. P. Abbott *et al.* (LIGO Scientific, Virgo), *Phys. Rev. Lett.* **119**, 161101 (2017).
- [14] C. M. Will, *Phys. Rev. D* **50**, 6058 (1994).
- [15] E. Barausse, C. Palenzuela, M. Ponce, and L. Lehner, *Phys. Rev. D* **87**, 081506 (2013), arXiv:1212.5053 [gr-qc].
- [16] B. P. Abbott *et al.* (LIGO Scientific, Virgo), *Phys. Rev. Lett.* **123**, 011102 (2019), arXiv:1811.00364 [gr-qc].
- [17] X. Zhang, J. Yu, T. Liu, W. Zhao, and A. Wang, *Phys. Rev. D* **95**, 124008 (2017), arXiv:1703.09853 [gr-qc].
- [18] J. Zhao, L. Shao, Y. Gao, C. Liu, Z. Cao, and B.-Q. Ma, (2021), arXiv:2106.04883 [gr-qc].
- [19] L. Shao, N. Sennett, A. Buonanno, M. Kramer, and N. Wex, *Phys. Rev. X* **7**, 041025 (2017).
- [20] D. Anderson, P. Freire, and N. Yunes, *Class. Quant. Grav.* **36**, 225009 (2019), arXiv:1901.00938 [gr-qc].
- [21] J. Zhao, L. Shao, Z. Cao, and B.-Q. Ma, *Phys. Rev. D* **100**, 064034 (2019), arXiv:1907.00780 [gr-qc].
- [22] M. Guo, J. Zhao, and L. Shao, (2021), arXiv:2106.01622 [gr-qc].
- [23] D. Anderson, N. Yunes, and E. Barausse, *Phys. Rev. D* **94**, 104064 (2016), arXiv:1607.08888 [gr-qc].



- [24] F. M. Ramazanoğlu and F. Pretorius, *Phys. Rev. D* **93**, 064005 (2016).
- [25] S. S. Yazadjiev, D. D. Doneva, and D. Popchev, *Phys. Rev. D* **93**, 084038 (2016).
- [26] J. Alsing, E. Berti, C. M. Will, and H. Zanglauer, *Phys. Rev. D* **85**, 064041 (2012), arXiv:1112.4903 [gr-qc].
- [27] T. Liu, W. Zhao, and Y. Wang, *Phys. Rev. D* **102**, 124035 (2020), arXiv:2007.10068 [gr-qc].
- [28] R. F. Mendes, *Phys. Rev. D* **91**, 064024 (2015).
- [29] R. Xu, Y. Gao, and L. Shao, *Phys. Rev. D* **102**, 064057 (2020), arXiv:2007.10080 [gr-qc].
- [30] D. S. Salopek, J. R. Bond, and J. M. Bardeen, *Phys. Rev. D* **40**, 1753 (1989).
- [31] H. Hu, M. Kramer, N. Wex, D. J. Champion, and M. S. Kehl, *Mon. Not. Roy. Astron. Soc.* **497**, 3118 (2020), arXiv:2007.07725 [astro-ph.SR].
- [32] H. O. Silva and N. Yunes, *Class. Quant. Grav.* **36**, 17LT01 (2019), arXiv:1902.10269 [gr-qc].
- [33] H. O. Silva and N. Yunes, *Phys. Rev. D* **99**, 044034 (2019).
- [34] H. Sotani, *Phys. Rev. D* **96**, 104010 (2017), arXiv:1710.10596 [astro-ph.HE].
- [35] M. C. Miller *et al.*, *Astrophys. J. Lett.* **918**, L28 (2021), arXiv:2105.06979 [astro-ph.HE].
- [36] G. Raaijmakers, S. K. Greif, K. Hebeler, T. Hinderer, S. Nissanke, A. Schwenk, T. E. Riley, A. L. Watts, J. M. Lattimer, and W. C. G. Ho, *Astrophys. J. Lett.* **918**, L29 (2021), arXiv:2105.06981 [astro-ph.HE].
- [37] R. Ciolfi *et al.*, (2021), arXiv:2104.09534 [astro-ph.IM].
- [38] T. Hinderer, *Astrophys. J.* **677**, 1216 (2008), arXiv:0711.2420 [astro-ph].
- [39] B. P. Abbott *et al.* (LIGO Scientific, Virgo), *Phys. Rev. X* **9**, 011001 (2019), arXiv:1805.11579 [gr-qc].
- [40] P. Pani and E. Berti, *Phys. Rev. D* **90**, 024025 (2014).
- [41] K. Yagi and N. Yunes, *Phys. Rev. D* **88**, 023009 (2013).
- [42] K. Yagi and N. Yunes, *Science* **341**, 365 (2013).
- [43] T. Damour, in *Physics of Relativistic Objects in Compact Binaries: From Birth to Coalescence*, Vol. 359, edited by M. Colpi, P. Casella, V. Gorini, U. Moschella, and A. Possenti (Springer, Dordrecht, 2009) p. 1, arXiv:0704.0749 [gr-qc].
- [44] D. M. Podkowka, R. F. P. Mendes, and E. Poisson, *Phys. Rev. D* **98**, 064057 (2018), arXiv:1807.01565 [gr-qc].
- [45] J. B. Hartle, *Astrophys. J.* **150**, 1005 (1967).
- [46] J. B. Hartle and K. S. Thorne, *Astrophys. J.* **153**, 807 (1968).
- [47] A. Akmal, V. R. Pandharipande, and D. G. Ravenhall, *Phys. Rev. C* **58**, 1804 (1998).
- [48] A. L. Watts *et al.*, *Rev. Mod. Phys.* **88**, 021001 (2016), arXiv:1602.01081 [astro-ph.HE].
- [49] S. Bogdanov, G. B. Rybicki, and J. E. Grindlay, *Astrophys. J.* **670**, 668 (2007), arXiv:astro-ph/0612791.
- [50] S. Bogdanov, J. E. Grindlay, and G. B. Rybicki, *Astrophys. J.* **689**, 407 (2008), arXiv:0801.4030 [astro-ph].
- [51] V. E. Zavlin, G. G. Pavlov, and Y. A. Shibano, *Astron. Astrophys.* **315**, 141 (1996), arXiv:astro-ph/9604072.
- [52] T. Damour and A. Nagar, *Phys. Rev. D* **80**, 084035 (2009).
- [53] T. Regge and J. A. Wheeler, *Phys. Rev.* **108**, 1063 (1957).
- [54] K. Yagi and N. Yunes, *Phys. Rept.* **681**, 1 (2017).
- [55] D. D. Doneva, S. S. Yazadjiev, K. V. Staykov, and K. D. Kokkotas, *Phys. Rev. D* **90**, 104021 (2014).
- [56] D. D. Doneva and S. S. Yazadjiev, *JCAP* **11**, 019 (2016), arXiv:1607.03299 [gr-qc].
- [57] R. B. Wiringa, V. Fiks, and A. Fabrocini, *Phys. Rev. C* **38**, 1010 (1988).
- [58] F. Douchin and P. Haensel, *Astron. Astrophys.* **380**, 151 (2001).
- [59] C. Breu and L. Rezzolla, *Mon. Not. Roy. Astron. Soc.* **459**, 646 (2016), arXiv:1601.06083 [gr-qc].
- [60] M. Minamitsuji and H. O. Silva, *Phys. Rev. D* **93**, 124041 (2016), arXiv:1604.07742 [gr-qc].